MODEL FORM CALIBRATION IN DRIFT-DIFFUSION SIMULATION USING FRACTIONAL DERIVATIVES

Yan Wang
School of Mechanical Engineering
Georgia Institute of Technology
Atlanta, GA 30332

ABSTRACT

In modeling and simulation, model-form uncertainty arises from the lack of knowledge and simplification during modeling process and numerical treatment for ease of computation. Traditional uncertainty quantification approaches are based on assumptions of stochasticity in real, reciprocal, or functional spaces to make them computationally tractable. This makes the prediction of important quantities of interest such as rare events difficult. In this paper, a new approach to capture model-form uncertainty is proposed. It is based on fractional calculus, and its flexibility allows us to model a family of non-Gaussian processes, which provides a more generic description of the physical world. A generalized fractional Fokker-Planck equation (fFPE) is used to describe the drift-diffusion processes under long-range correlations and memory effects. A new model calibration approach based on the maximum mutual information is proposed to reduce model-form uncertainty, where an optimization procedure is taken.

1. INTRODUCTION

Two types of uncertainty are recognized in modeling and simulation. Aleatory uncertainty is due to pure randomness of physical world, whereas epistemic uncertainty is because of the lack of complete knowledge about the world. The major component of epistemic uncertainty is model-form uncertainty, which arises from the simplification during modeling process and numerical treatment for ease of computation. During the abstraction procedure, truncation is always applied to make simulation and computation tractable. As a result, error or bias is introduced. The difference between the model prediction of a quantity of interest (QoI) and its true value in the real physical world is the accumulative effect of model-form uncertainty and other input uncertainties such as variability and bias in the parameters and variables.

Classical uncertainty quantification (UQ) methods to model output uncertainty propagated from inputs, such as generalized polynomial chaos [1], moment and characteristic function [2], have relatively restrictive assumptions of stochasticity, i.e. the types of distributions to sample and the forms of polynomials in expansion. These methods are very effective in analyzing systems with low-dimensional parameter space that follow simple physics. However, when we are interested in multi-physics systems with nonlocal long-range correlations and memory effects, or extreme events under heavy-tailed distributions, these UQ methods can lead to inaccurate conclusion because the distributions have the bias toward traditional Gaussian process. The error is largely due to the selected model form. Although methods such as Bayesian model average are available to calibrate the model, they rely on the assumptions that all possible models and the corresponding probabilities that the models are correct are readily available.

In this paper, a new UQ method is proposed to describe multi-physics systems with model-form uncertainty incorporated, where the physics does not follow traditional partial differential equation (PDEs) or ordinary differential equations (ODEs). It is based on the concept of fractional calculus. Fractional calculus [3, 4] is a generalization of classical real analysis by introducing non-integer power and differentiation operators. As a result, classical differentiation equations that model system dynamics can be extended to fractional differentiation equations with fractional derivatives defined. Fractional calculus has been applied in the regimes of system dynamics and control [5, 6], signal processing [7], mechanics of quasi-brittle materials [8], non-local continuum and viscoelastic mechanics [9], space-time fractional diffusion equation [10, 11, 12], characterizing probability distributions with complex fractional moments [13, 14, 15, 16, 17], and fractional Schrödinger equation [18]. The uniqueness of fractional diffusion equation is that the solution can be deviated from the Gaussian process as in traditional diffusion equation. Therefore, heavy tails as in Lévy α-stable white noise processes can be obtained. Similarly, fractional Fokker-Planck equation with fractional derivatives models Lévy flights. Fractional Schrödinger equation generalizes the classical description of quantum system dynamics with Lévy stochastic process.

Based on fractional calculus, a generalized fractional Fokker-Planck equation is proposed in this paper to describe the general drift-diffusion process with multi-physics complexity. This approach does not need the assumption of the possible choices of models and associated probabilities. Rather, the form of model may vary dynamically based on the control of several parameters. In other words, the model form may change parametrically during simulation.

In addition, the flexibility of the fractional Fokker-Planck equation allows us to represent the evolution of probability distributions with heavy tails, since the results of fractional calculus can be geometrically interpreted as fractals, physically as long-range interaction or long-term memory, and probabilistically as heavy-tailed stable distributions. Rare event with extreme impact has been a classical interest in statistics. Extreme value distribution functions [19,20] (e.g. Fréchet, Gumbel, and negative Weibull) are typically used in modeling long tails. Yet, they are general enough to capture the variation of the distribution form. In this paper, a new model calibration approach is proposed to reduce model-form uncertainty. It is based on the mechanism of maximizing a new criterion, accumulative mutual information, such that the accumulative difference between the target distribution and the predicted probability evolution from the fractional Fokker-Planck equation is minimized.

In the remainder of the paper, the application of fractional calculus in diffusion is introduced in Section 2. The generalized fractional Fokker-Planck equation is proposed and the analytical solution is provided in Section 3. The sensitivity analysis based on the analytical solution for drift-diffusion processes is presented in Section 4.1. The new model calibration approach is described in Section 4.2.

2. FRACTIONAL DERIVATIVES AND FRACTIONAL DRIFT-DIFFUSION

Several forms of fractional integrals and derivatives have been developed. The definitions of left and right Riemann-Liouville fractional integrals are

$$D_{+}^{-\alpha} f(x) = \frac{1}{\Gamma(\alpha)} \int_{-\infty}^{x} (x-\xi)^{\alpha-1} f(\xi) d\xi \tag{1}$$

and

$$D_{-}^{-\alpha} f(x) = \frac{1}{\Gamma(\alpha)} \int_{x}^{+\infty} (\xi-x)^{\alpha-1} f(\xi) d\xi \tag{2}$$

respectively.

The definitions of left and right Riemann-Liouville fractional derivatives are

$$D_{+}^{\alpha} f(x) = \frac{1}{\Gamma(n-\alpha)} \frac{d^n}{dx^n} \int_{-\infty}^{x} (x-\xi)^{n-\alpha-1} f(\xi) d\xi \tag{3}$$

and

$$D_{-}^{\alpha} f(x) = \frac{(-1)^n}{\Gamma(n-\alpha)} \frac{d^n}{dx^n} \int_{x}^{+\infty} (\xi - x)^{n-\alpha-1} f(\xi) d\xi \tag{4}$$

where integer $n = \lfloor \alpha \rfloor$ or $n \le \alpha < n+1$.

The Riesz fractional integral is defined as

$$D^{-\alpha} f(x) = \frac{1}{2\cos(\alpha\pi/2)} [D_{+}^{-\alpha} f(x) + D_{-}^{-\alpha} f(x)] \tag{5}$$

and the Riesz fractional derivative is defined as .

$$D^{\alpha} f(x) = -\frac{1}{2\cos(\alpha\pi/2)} [D_{+}^{\alpha} f(x) + D_{-}^{\alpha} f(x)] \tag{6}$$

The Fourier transform of Riemann-Liouville and Riesz fractional derivatives are

$$\mathcal{F}\{D_{\pm}^{\alpha} f(x); k\} = (\mp ik)^{\alpha} \mathcal{F}\{f(x); k\} \tag{7}$$

and

$$\mathcal{F}\{D^{\alpha} f(x); k\} = -|k|^{\alpha} \mathcal{F}\{f(x); k\} \tag{8}$$

respectively with $\alpha > 0$ and $i^2 = -1$, where

$$\mathcal{F}\{f(x); k\} = \hat{f}(k) = \int_{-\infty}^{+\infty} e^{ikx} f(x) dx \quad (k \in \mathbb{R}) \tag{9}$$

and

$$\mathcal{F}^{-1}\{\hat{f}(k); x\} = f(x) = \frac{1}{2\pi} \int_{-\infty}^{+\infty} e^{-ikx} \hat{f}(k) dk \quad (x \in \mathbb{R}) \tag{10}$$

Notice that

$$(\mp ik)^{\alpha} = |k|^{\alpha} e^{\mp i \,\mathrm{sgn}(k) \alpha\pi/2} \tag{11}$$

and $\mathrm{sgn}(x) = 1$ if $x > 0$, $\mathrm{sgn}(x) = 0$ if $x = 0$, and $\mathrm{sgn}(x) = -1$ if $x < 0$.

Analogously, the Fourier transforms of Riemann-Liouville and Riesz fractional integrals are given by

$$\mathcal{F}\{D_{\pm}^{-\alpha} f(x); k\} = (\mp ik)^{-\alpha} \mathcal{F}\{f(x); k\} \quad (0 < \alpha < 1) \tag{12}$$

$$\mathcal{F}\{D^{-\alpha} f(x); k\} = |k|^{-\alpha} \mathcal{F}\{f(x); k\} \quad (0 < \alpha < 1) \tag{13}$$

For order $0 < \alpha \le 2$ and skewness $|\theta| \le \min(\alpha, 2-\alpha)$, the Riesz-Feller derivative is defined as

$${}_{x}D_{\theta}^{\alpha} f(x) = \frac{\Gamma(1+\alpha)}{\pi} \left\{ \begin{aligned} &\sin\frac{(\alpha+\theta)\pi}{2} \int_{0}^{\infty} \frac{f(x+\xi) - f(x)}{\xi^{1+\alpha}} d\xi \\ &+ \sin\frac{(\alpha-\theta)\pi}{2} \int_{0}^{\infty} \frac{f(x-\xi) - f(x)}{\xi^{1+\alpha}} d\xi \end{aligned} \right\} \tag{14}$$

so that its Fourier transform is

$$\mathcal{F}\{{}_{x}D_{\theta}^{\alpha} f(x); k\} = -|k|^{\alpha} e^{i \,\mathrm{sgn}(k) \theta\pi/2} \mathcal{F}\{f(x); k\} \quad (0 < \alpha \le 2) \tag{15}$$

The Caputo fractional derivative of order γ, with $m-1 < \gamma \le m$ and m as an integer, is defined as

$$ {}_tD_*^{\gamma} f(t) = \begin{cases} \dfrac{d^m}{dt^m}\left[\dfrac{1}{\Gamma(m-\gamma)}\displaystyle\int_0^t (t-\tau)^{m-1-\gamma} f(\tau)d\tau\right] & (m-1<\gamma<m) \\ \dfrac{d^m}{dt^m} f(t) & (\gamma = m) \end{cases} \tag{16} $$

Its Laplace transform is

$$ \mathcal{L}\{{}_tD_*^{\gamma} f(t);s\} = s^{\gamma}\tilde{f}(s) - \sum_{k=0}^{m-1} s^{\gamma-1-k}\tilde{f}(0^+) \tag{17} $$

Different versions of fractional Fokker-Planck equation (fFPE) have been proposed. Wyss [21] introduced time fractional derivative into the diffusion equation. Fogedby [10] introduced a fractional diffusion term as a spatially nonlocal integral operator into the original FPE to model lévy flights and long-range steps. Meerschaert et al. [22, 23] used the Riesz fractional derivative in the diffusion term of spatial fFPE. Metzler et al. [24] applied the Riesz fractional derivative to the spatial diffusion term and the left Riemann-Liouville fractional derivative to time. Mainardi et al. [11] formulated the space-time fFPE with the Caputo fractional derivative in Eq.(16) for time derivative with $0<\gamma\le 1$ and the Riesz-Feller derivative in Eq.(14) for the diffusion term with $0<\alpha\le 2$. Liu et al. [25] applied fractional time derivative to FPE. Huang and Liu [26] extended the space-time fFPE by inserting the traditional drift term with the integer order derivative back to the equation. Liu et al. [27] further generalized with the left Riemann-Liouville fractional derivatives for both drift and diffusion, in addition to the Caputo fractional derivative for time. Yıldırım and Koçak [28] introduced the fractional order of drift as a half of the fraction order of diffusion.

Different methods were also developed to solve fFPEs. Fox functions [21] were applied to find analytical solutions of fractional diffusion problems. Finite difference approximation [29, 27] can be applied to either space, time, or both, and the solving process is similar to the one for ordinary differential equations. Homotopy perturbation method [30, 28] approximates solutions analytically. Fourier transform [23, 31] and Mellin transform [32] can be applied to space fFPEs. Similarly Laplace transform [25] can be applied to time fFPEs. Both Fourier and Laplace transforms [11, 26] are needed for space-time fFPEs.

3. FRACTIONAL FOKKER-PLANCK EQUATION FOR DRIFT-DIFFUSION MODEL

The fFPE proposed here is

$$ {}_tD_*^{\gamma} p(x,t) = -K_{\alpha} D_+^{\alpha} p(x,t) + K_{\beta}\,{}_xD_{\theta}^{\beta} p(x,t) \tag{18} $$

is a generalization of classical drift-diffusion equation that describes drift-diffusion processes, where $p(x,t)$ is the probability that a particle is found at x at time t or the spatial distribution of fluid density or solute concentration at a particular time. K_{α} and K_{β} are the respective coefficients for drift and diffusion. In addition, $0<\alpha\le 1$ and $1<\beta\le 2$ are the fractional orders of spatial derivatives, $0<\gamma\le 1$ is the fractional order of temporal derivative. As a result,

$$ D_+^{\alpha} p(x,t) = \frac{1}{\Gamma(1-\alpha)}\frac{d}{dx}\int_{-\infty}^{x} (x-\xi)^{-\alpha} p(\xi,t)d\xi \tag{19} $$

Also on the right hand side of Eq.(18), ${}_xD_{\theta}^{\beta}$ is the Riesz-Feller derivative of order β. On the left side of Eq.(18),

Note that the fFPE proposed here includes an independent fractional drift term in addition to the fractional diffusion term, which is slightly different from the fFPEs in Refs.[27, 28]. The fractional order diffusion is observed as subdiffusive or superdiffusive phenomena, and the

fractional order time derivative is used to model memory effects. The fractional order drift is considered as the spatial effect of external velocity or force fields in anomalous diffusion, which introduces heterogeneity of advection or drift. The introduction of fractional order parameters increases the flexibility of FPEs.

Applying Laplace transform to both sides of Eq.(18), we receive

$$s^{\gamma}\tilde{p}(x,s)-s^{\gamma-1}\tilde{p}(x,0)=-K_{\alpha}D^{\alpha}\tilde{p}(x,s)+K_{\beta}{}_{x}D_{\theta}^{\beta}\tilde{p}(x,s) \tag{20}$$

Applying Fourier transform further to both sides of Eq.(20) yields

$$s^{\gamma}\hat{\tilde{p}}(k,s)-s^{\gamma-1}\hat{\tilde{p}}(k,0)=-K_{\alpha}(-ik)^{\alpha}\hat{\tilde{p}}(k,s)+K_{\beta}\mid k\mid^{\beta}\ e^{i\,\mathrm{sgn}(k)\theta\pi/2}\hat{\tilde{p}}(k,s) \tag{21}$$

Therefore,

$$\hat{\tilde{p}}(k,s)=\frac{s^{\gamma-1}}{s^{\gamma}-(K_{\beta}\mid k\mid^{\beta}\ e^{i\,\mathrm{sgn}(k)\theta\pi/2}-K_{\alpha}(-ik)^{\alpha})}\hat{\tilde{p}}(k,0) \tag{22}$$

The inverse Laplace transform of Eq.(22) is

$$\hat{p}(k,t)=\mathcal{E}_{\gamma,1}(K_{\beta}\mid k\mid^{\beta}\ e^{i\,\mathrm{sgn}(k)\theta\pi/2}t^{\gamma}-K_{\alpha}(-ik)^{\alpha}t^{\gamma})\hat{p}(k,0) \tag{23}$$

where $\mathcal{E}_{\gamma,1}$ is the Mittag-Leffler function of order $(\gamma,1)$. The general Mittag-Leffler function of order (γ,η) is defined as

$$\mathcal{E}_{\gamma,\eta}(z)=\sum_{n=0}^{\infty}\frac{z^{n}}{\Gamma(\gamma n+\eta)} \tag{24}$$

The inverse Fourier transform of Eq.(23) is

$$\begin{aligned}
p(x,t)&=\frac{1}{2\pi}\int_{-\infty}^{+\infty}e^{-ikx}\mathcal{E}_{\gamma,1}(K_{\beta}\mid k\mid^{\beta}\ e^{i\,\mathrm{sgn}(k)\theta\pi/2}t^{\gamma}-K_{\alpha}(-ik)^{\alpha}t^{\gamma})\hat{p}(k,0)dk\\
&=\frac{1}{2\pi}\int_{-\infty}^{+\infty}e^{-ikx}\mathcal{E}_{\gamma,1}(K_{\beta}\mid k\mid^{\beta}\ e^{i\,\mathrm{sgn}(k)\theta\pi/2}t^{\gamma}-K_{\alpha}(-ik)^{\alpha}t^{\gamma})\int_{-\infty}^{+\infty}e^{iky}p(y,0)dydk\\
&=\int_{-\infty}^{+\infty}\frac{1}{2\pi}\int_{-\infty}^{+\infty}e^{-ik(x-y)}\mathcal{E}_{\gamma,1}(K_{\beta}\mid k\mid^{\beta}\ e^{i\,\mathrm{sgn}(k)\theta\pi/2}t^{\gamma}-K_{\alpha}(-ik)^{\alpha}t^{\gamma})dkp(y,0)dy\\
&=\int_{-\infty}^{+\infty}G_{\alpha,\beta,\gamma}^{\theta}(x-y,t)p(y,0)dy\\
&=G_{\alpha,\beta,\gamma}^{\theta}(x,t)\otimes p(y,0)
\end{aligned} \tag{25}$$

where

$$G_{\alpha,\beta,\gamma}^{\theta}(x,t)=\frac{1}{2\pi}\int_{-\infty}^{+\infty}e^{-ikx}\mathcal{E}_{\gamma,1}(-K_{\alpha}(-ik)^{\alpha}t^{\gamma}+K_{\beta}\mid k\mid^{\beta}\ e^{i\,\mathrm{sgn}(k)\theta\pi/2}t^{\gamma})dk \tag{26}$$

is the Green or kernel function. Its Fourier transform is

$$\hat{G}_{\alpha,\beta,\gamma}^{\theta}(k,t)=\mathcal{E}_{\gamma,1}(-K_{\alpha}(-ik)^{\alpha}t^{\gamma}+K_{\beta}\mid k\mid^{\beta}\ e^{i\,\mathrm{sgn}(k)\theta\pi/2}t^{\gamma}) \tag{27}$$

The analytical solution in Eq.(25) for fFPE can be approximated by continuous-time random walk or path integrals. Notice that the kernel function in Eq.(26) is a generalization of traditional Gaussian kernel. When $\alpha=1$, $\beta=2$, $\gamma=1$, and $\theta=0$, the kernel function becomes Gaussian.

The fFPE in Eq.(18) provides a parametric approach to represent model-form uncertainty. Different combinations of α, β, γ, and θ lead to distributions with heavy tails or skewness. Orders α and β capture the uncertainty related to spatial distribution, whereas γ provides the sense of uncertainty in time domain. Skewness θ represents the anisotropic property of diffusion so that dispersion is orientation-dependent.

To provide a sense of how the parameters affect the simulation results, here some plots of probability density functions (pdf's) with different model-form parameters are given. Figure 1 shows the effect of skewness θ, and Figure 2 illustrates the effect of β. It is seen that θ provides

skewness of distributions with direction determined by its sign. A smaller diffusion order β indicates a slower diffusion process. The effect of fractional order α is further shown in Figure 3, where smaller α damps the influence of external field on drift process. The effect of time fractional order γ is illustrated in Figure 4. Small orders of γ lead to long-tailed distributions, which captures the slowly decaying memory effect.

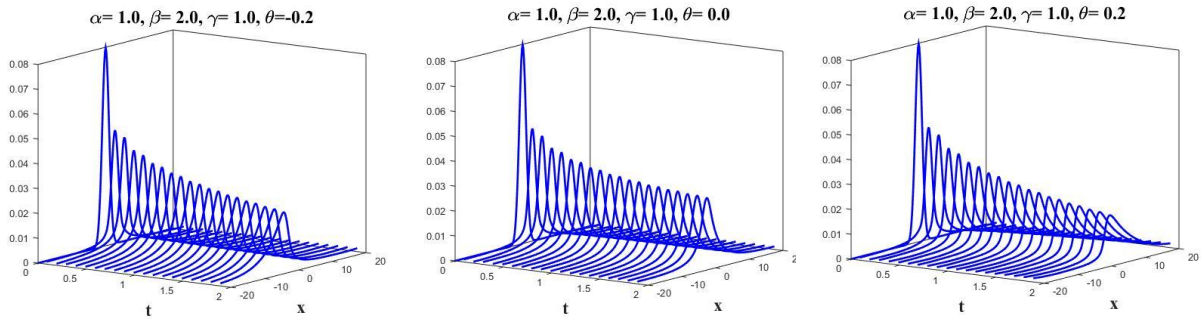

(a) (b) (c)

Figure 1: The effect of skewness θ on probability density functions

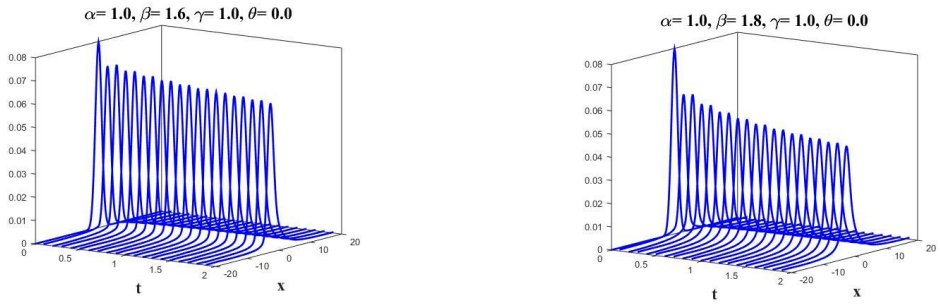

(a) (b)

Figure 2: The effect of β on probability density functions

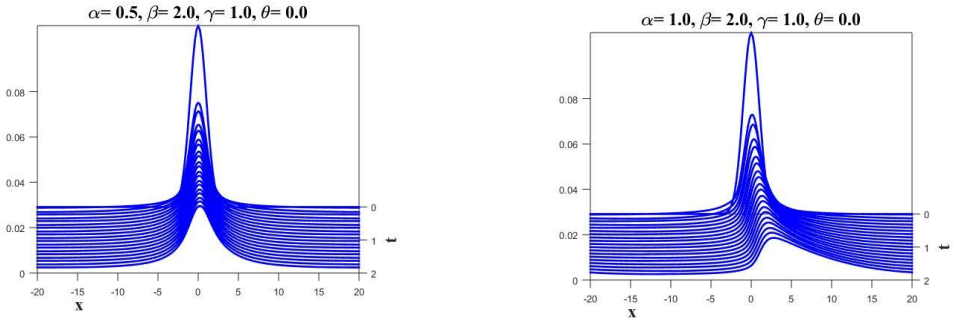

(a) (b)

Figure 3: The effect of α on probability density functions

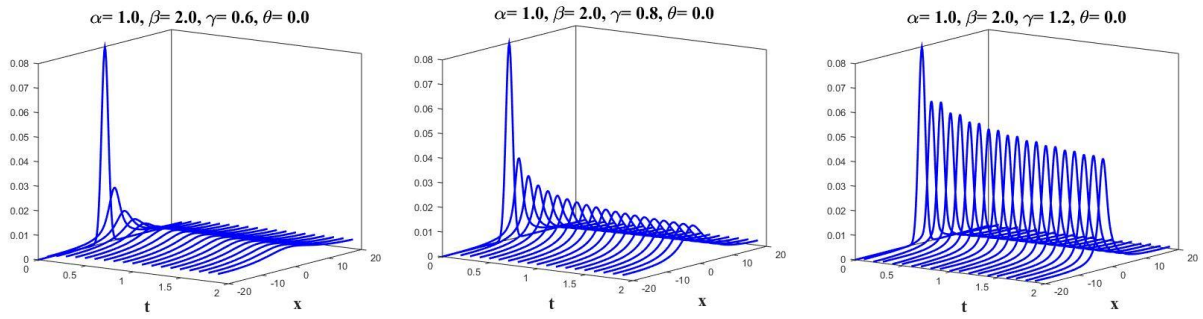

(a) (b) (c)

Figure 4: The effect γ on probability density functions

4. QUANTIFICATION OF MODEL-FORM UNCERTAINTY IN DRIFT-DIFFUSION PROCESSES

As shown in Section 3, model-form parameters α, β, γ, and θ provide a variety of possible probability distributions which cannot be obtained by simply changing drift and diffusion coefficients of classical FPE. The flexibility provides a new approach to quantify model-form uncertainty. In this section, a new approach of model selection based on calibration is proposed, where an optimization formulation is developed to reduce model-form uncertainty. It uses the local sensitivity analysis of model prediction with different model forms.

4.1 Local Sensitivity Analysis

For global sensitivity analysis, we may choose statistical [33] or non-statistical [34] approaches. Here, the local sensitivity of the model prediction in Eq.(25) is analyzed by estimating the first derivatives with respect to the model-form parameters.

If the probability in Eq.(25) is denoted as $P(x,t \mid \Lambda)$ where $\Lambda = (\alpha, \beta, \gamma, \theta)$ is the combination of model-form parameters, then

$$\begin{aligned} \frac{\partial}{\partial \Lambda} P(x,t \mid \Lambda) &= \frac{\partial}{\partial \Lambda} G^{\theta}_{\alpha,\beta,\gamma}(x) \otimes p(y,0) \\ &= \int_{-\infty}^{+\infty} \frac{\partial}{\partial \Lambda} G^{\theta}_{\alpha,\beta,\gamma}(x-y,t) p(y,0) dy \end{aligned} \tag{28}$$

Specifically,

$$\frac{\partial}{\partial \alpha} G^{\theta}_{\alpha,\beta,\gamma}(x,t) = \frac{1}{2\pi} \int_{-\infty}^{+\infty} e^{-ikx} \frac{-\alpha K_{\alpha} (-ik)^{\alpha-1}}{\gamma(-K_{\alpha}(-ik)^{\alpha} + K_{\beta} \mid k \mid^{\beta} e^{i\,\mathrm{sgn}(k)\theta\pi/2})} \mathcal{E}_{\gamma,0}(-K_{\alpha}(-ik)^{\alpha} t^{\gamma} + K_{\beta} \mid k \mid^{\beta} e^{i\,\mathrm{sgn}(k)\theta\pi/2} t^{\gamma}) dk \tag{29}$$

$$\frac{\partial}{\partial \beta} G^{\theta}_{\alpha,\beta,\gamma}(x,t) = \frac{1}{2\pi} \int_{-\infty}^{+\infty} e^{-ikx} \frac{\beta K_{\beta} \mid k \mid^{\beta-1} e^{i\,\mathrm{sgn}(k)\theta\pi/2}}{\gamma(-K_{\alpha}(-ik)^{\alpha} + K_{\beta} \mid k \mid^{\beta} e^{i\,\mathrm{sgn}(k)\theta\pi/2})} \mathcal{E}_{\gamma,0}(-K_{\alpha}(-ik)^{\alpha} t^{\gamma} + K_{\beta} \mid k \mid^{\beta} e^{i\,\mathrm{sgn}(k)\theta\pi/2} t^{\gamma}) dk \tag{30}$$

$$\frac{\partial}{\partial \gamma} G^{\theta}_{\alpha,\beta,\gamma}(x,t) = \frac{1}{2\pi} \int_{-\infty}^{+\infty} e^{-ikx} t^{-1} \mathcal{E}_{\gamma,0}(-K_{\alpha}(-ik)^{\alpha} t^{\gamma} + K_{\beta} \mid k \mid^{\beta} e^{i\,\mathrm{sgn}(k)\theta\pi/2} t^{\gamma}) dk \tag{31}$$

$$\frac{\partial}{\partial \theta} G^{\theta}_{\alpha,\beta,\gamma}(x,t) = \frac{1}{2\pi} \int_{-\infty}^{+\infty} e^{-ikx} \frac{i\,\mathrm{sgn}(k) \frac{\pi}{2} K_{\beta} \mid k \mid^{\beta} e^{i\,\mathrm{sgn}(k)\theta\pi/2}}{\gamma(-K_{\alpha}(-ik)^{\alpha} + K_{\beta} \mid k \mid^{\beta} e^{i\,\mathrm{sgn}(k)\theta\pi/2})} \mathcal{E}_{\gamma,0}(-K_{\alpha}(-ik)^{\alpha} t^{\gamma} + K_{\beta} \mid k \mid^{\beta} e^{i\,\mathrm{sgn}(k)\theta\pi/2} t^{\gamma}) dk \tag{32}$$

The respective Fourier transforms are

$$\mathcal{F}\{\frac{\partial}{\partial\alpha}G^{\theta}_{\alpha,\beta,\gamma}(x,t);k\} = \frac{-\alpha K_{\alpha}(-ik)^{\alpha-1}}{\gamma(-K_{\alpha}(-ik)^{\alpha} + K_{\beta} \mid k \mid^{\beta} e^{i\,\mathrm{sgn}(k)\theta\pi/2})}\mathcal{E}_{\gamma,0}(-K_{\alpha}(-ik)^{\alpha}t^{\gamma} + K_{\beta} \mid k \mid^{\beta} e^{i\,\mathrm{sgn}(k)\theta\pi/2}t^{\gamma}) \tag{33}$$

$$\mathcal{F}\{\frac{\partial}{\partial\beta}G^{\theta}_{\alpha,\beta,\gamma}(x,t);k\} = \frac{\beta K_{\beta} \mid k \mid^{\beta-1} e^{i\,\mathrm{sgn}(k)\theta\pi/2}}{\gamma(-K_{\alpha}(-ik)^{\alpha} + K_{\beta} \mid k \mid^{\beta} e^{i\,\mathrm{sgn}(k)\theta\pi/2})}\mathcal{E}_{\gamma,0}(-K_{\alpha}(-ik)^{\alpha}t^{\gamma} + K_{\beta} \mid k \mid^{\beta} e^{i\,\mathrm{sgn}(k)\theta\pi/2}t^{\gamma}) \tag{34}$$

$$\mathcal{F}\{\frac{\partial}{\partial\gamma}G^{\theta}_{\alpha,\beta,\gamma}(x,t);k\} = t^{-1}\mathcal{E}_{\gamma,0}(-K_{\alpha}(-ik)^{\alpha}t^{\gamma} + K_{\beta} \mid k \mid^{\beta} e^{i\,\mathrm{sgn}(k)\theta\pi/2}t^{\gamma}) \tag{35}$$

$$\mathcal{F}\{\frac{\partial}{\partial\theta}G^{\theta}_{\alpha,\beta,\gamma}(x,t);k\} = \frac{i\,\mathrm{sgn}(k)\frac{\pi}{2}K_{\beta} \mid k \mid^{\beta} e^{i\,\mathrm{sgn}(k)\theta\pi/2}}{\gamma(-K_{\alpha}(-ik)^{\alpha} + K_{\beta} \mid k \mid^{\beta} e^{i\,\mathrm{sgn}(k)\theta\pi/2})}\mathcal{E}_{\gamma,0}(-K_{\alpha}(-ik)^{\alpha}t^{\gamma} + K_{\beta} \mid k \mid^{\beta} e^{i\,\mathrm{sgn}(k)\theta\pi/2}t^{\gamma}) \tag{36}$$

Notice that [35]

$$\frac{d}{dz}\mathcal{E}_{\gamma,\eta}(z) = \frac{\mathcal{E}_{\gamma,\eta-1}(z) - (\eta-1)\mathcal{E}_{\gamma,\eta}(z)}{\gamma z}$$

Therefore,

$$\frac{d}{dz}\mathcal{E}_{\gamma,1}(z) = \frac{\mathcal{E}_{\gamma,0}(z)}{\gamma z}$$

The sensitivity formulation is used in the calibration process described in the following section.

4.2 Model Form Calibration

Here a new approach for model calibration is proposed, which is based on mutual information. Given two random variables X and Y, the mutual information of the two variables is defined as

$$I(X,Y) = \int\int p(X,Y)\log\frac{p(X,Y)}{p(X)p(Y)}\,dXdY \tag{37}$$

The new calibration process is based on the criteria of the maximum accumulative mutual information between the model prediction and experimental observation. Given the model prediction $p(x,t)$ from a particular form and the observation $p(z,t)$ from experiment, the *accumulative mutual information* between the two is defined as

$$\mathcal{M}(x,z) = \int\int\int p(x,z,t)\log\frac{p(x,z,t)}{p(x,t)p(z,t)}\,dxdzdt \tag{38}$$

where the joint probability

$$p(x,z,t) = p(z \mid x,t)p(x,t) \tag{39}$$

Here, the likelihood $p(x \mid z,t)$ characterizes the difference between the observation and model prediction. The likelihood is

$$\begin{aligned} p(z \mid x,t) &= \int_{-\infty}^{+\infty} G^{\theta}_{\alpha,\beta,\gamma}((x-z)-y,t)p(y,0)dy \\ &= G^{\theta}_{\alpha,\beta,\gamma}(x-z)\otimes p(y,0) \\ &= P(x-z,t \mid \Lambda) \end{aligned} \tag{40}$$

The proposed criteria for model calibration is to find the optimum parameters α, β, γ, and θ as the solution of

$$\max_{\alpha,\beta,\gamma,\theta}\mathcal{M}(x,z) \tag{41}$$

Given Eqs.(25) and (39), the accumulative mutual information in Eq.(38) becomes

$$\begin{aligned}
&\mathcal{M}(x,z)\\
&=\iiint p(z\mid x,t)p(x,t)\log\frac{p(z\mid x,t)}{p(z,t)}\,dxdzdt\\
&=\iiint\left[\log\frac{\begin{matrix}G^{\theta}_{\alpha,\beta,\gamma}(x-z,t)\otimes p(y,0) & G^{\theta}_{\alpha,\beta,\gamma}(x,t)\otimes p(y,0)\\ G^{\theta}_{\alpha,\beta,\gamma}(x-z,t)\otimes p(y,0)\end{matrix}}{p(z,t)}\right]dxdzdt\\
&=\iiint\left[P(x-z,t\mid\Lambda)P(x,t\mid\Lambda)\log\frac{P(x-z,t\mid\Lambda)}{p(z,t)}\right]dxdzdt
\end{aligned}\tag{42}$$

The local search direction to find the optimum solution of Eq.(41) is the first derivative of Eq.(42) with respect to the model-form parameters, which is

$$\begin{aligned}
&\frac{\partial}{\partial\Lambda}\mathcal{M}(x,z)\\
&=\iiint\left[\begin{matrix}P(x,t\mid\Lambda)\left[1+\log\dfrac{P(x-z,t\mid\Lambda)}{p(z,t)}\right]\dfrac{\partial}{\partial\Lambda}P(x-z,t\mid\Lambda)\\ +P(x-z,t\mid\Lambda)\log\dfrac{P(x-z,t\mid\Lambda)}{p(z,t)}\dfrac{\partial}{\partial\Lambda}P(x,t\mid\Lambda)\end{matrix}\right]dxdzdt
\end{aligned}\tag{43}$$

Notice that

$$\frac{\partial}{\partial\Lambda}P(x-z,t\mid\Lambda)=\frac{\partial}{\partial\Lambda}G^{\theta}_{\alpha,\beta,\gamma}(x-z)\otimes p(y,0)\tag{44}$$

which is similar to Eq.(28). The calibration process will follow the algorithm of optimization in Table 1. A simplified version of calibration is obviously based on mutual information instead of accumulative mutual information in Eq.(38).

A numerical example is used to demonstrate the proposed calibration procedure. 2,000 samples are randomly drawn from a Gaussian distribution. The simpler criterion of maximizing mutual information is applied. The histogram of experimental data is shown in Figure 5(a). An initial set of parameters ($\alpha=1$, $\beta=1.9$, $\gamma=0.8$, and $\theta=0.4$) are first given and the corresponding pdf is shown as the dash line in Figure 5(a). After 137 iterations of searching procedure in the algorithm in Table 1, the updated and final pdf are shown as the solid lines in Figure 5(a). The optimized parameters are $\alpha=1$, $\beta=1.901$, $\gamma=1.147$, and $\theta=0.741$. The search histories of γ and θ are shown in Figure 5(b) and (c) respectively. The value of mutual information gradually increases until it converges, as shown in Figure 6.

Table 1: The algorithm of model calibration

1.	Provide the distribution $p(z,t)$ from observation data;
2.	Provide an initial guess of Λ ;
3.	Calculate $P(x,t\mid\Lambda)$ based on Eq.(25);
4.	Calculate $P(x-z,t\mid\Lambda)$ based on Eq.(40);
5.	Calculate $\partial\mathcal{M}\,/\,\partial\Lambda$ based on Eq.(43);
6.	IF $\mid\partial\mathcal{M}\,/\,\partial\Lambda\mid>\varepsilon$
7.	Choose a step size λ , $\Lambda\leftarrow\Lambda+\lambda(\partial\mathcal{M}\,/\,\partial\Lambda)$;
8.	Go to Step 3;
9.	ELSE
10.	Stop.

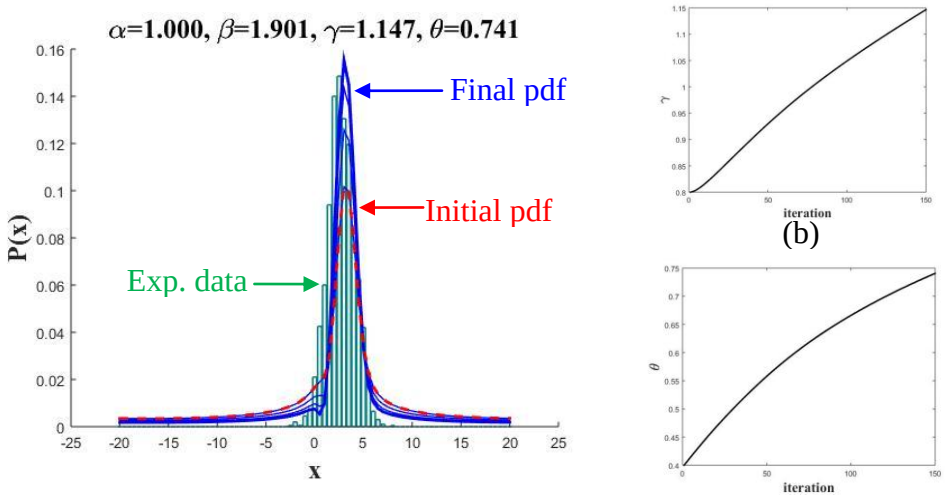

(a) (b) (c)

Figure 5: The search history of model-form parameters in the calibration process against random samples from a Gaussian distribution. (a) pdf evolution. (b) γ. (c) θ.

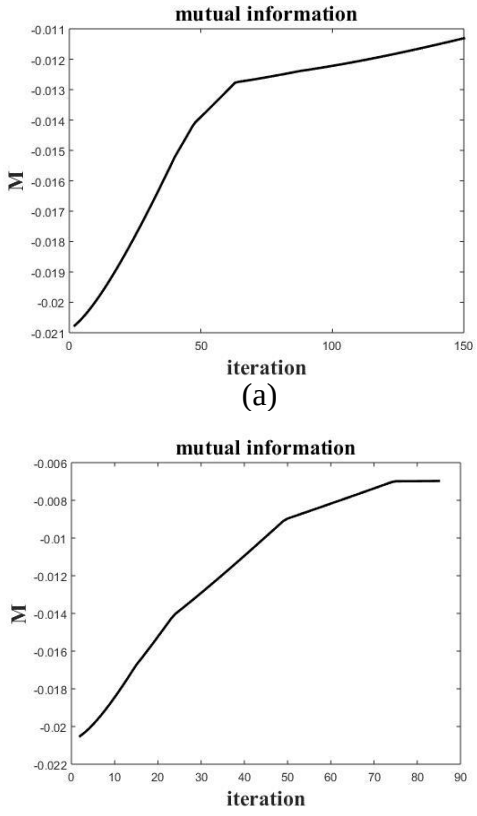

(a)

(b)

Figure 6: The search history of mutual information with different step sizes for Gaussian distribution. (a) step size λ = 1.0. (b) step size λ = 2.0.

Notice that the number of iterations is directly related to the threshold value ε in the stop criteria as well as the step size λ during the search. The threshold value used in Figure 6(a) is 5e−6 and the step size is 1.0. A larger threshold value or a larger step size will lead to fewer iterations. For instance, when the step size is increased to 2.0, the number of iterations is reduced to 87 with the same threshold value, as shown in Figure 6(b).

The proposed calibration approach can also be applied dynamically as an incremental calibration procedure when data are collected sequentially and the model can be re-estimated accordingly.

Compared to Bayesian model average, there is no need to assume the probabilities associated with different model choices. The calibration process is continuous for model-form parameters.

The second example is to calibrate the model against a Fréchet distribution with the pdf as

$$f(x) = \begin{cases} 0 & (x < \mu - \frac{\sigma}{\xi}) \\ \sigma^{-1}[1+\xi(\frac{x-\mu}{\sigma})]^{-1-1/\xi} \exp\{-[1+\xi(\frac{x-\mu}{\sigma})]^{-1/\xi}\} & otherwise \end{cases}$$

with parameters $\mu = 0.0$, $\sigma = 1.0$, and $\xi = 0.5$. The result of calibration is shown in Figure 7, where the solid line with star markers denotes the pdf of Fréchet distribution, the dash line is the initial pdf, and the solid lines show the update process of calibrated pdf. The change of mutual information is shown in Figure 8.

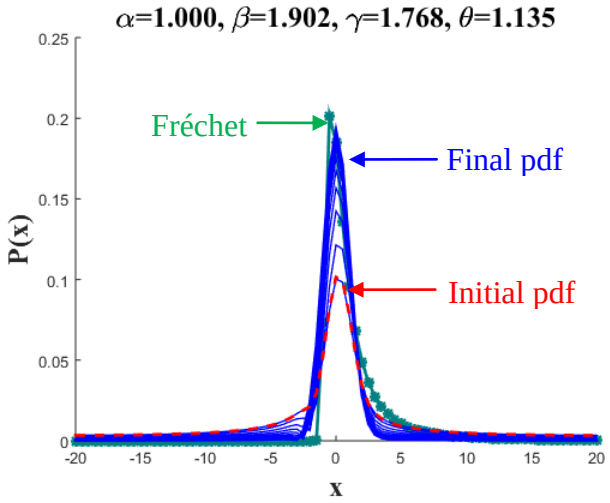

Figure 7: pdf evolved in the calibration process against a Fréchet distribution

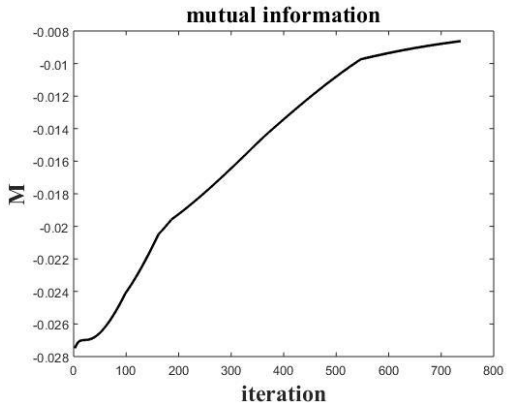

Figure 8: The search history of mutual information for Fréchet distribution

A third numerical example is the calibration process based on 2,000 samples randomly drawn from a lognormal distribution with $\mu = 1.0$ and $\sigma = 1.0$. The result is shown in Figure 9.

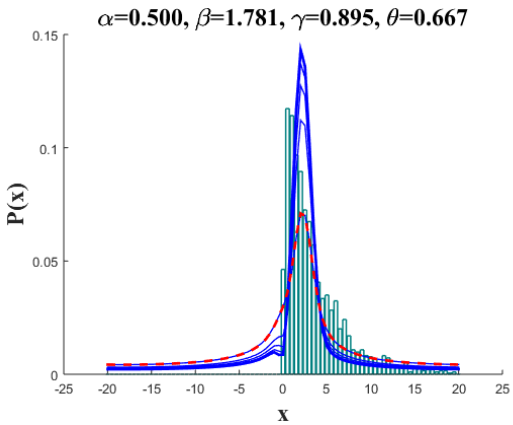

Figure 9: pdf evolved in the calibration process against random samples from a lognormal distribution

In the above three examples, only one-step mutual information was applied. If accumulative mutual information is used, the model is calibrated based on the complete history of pdf evolution simultaneously. Figure 10 shows such an example, where histograms for three time steps (t=0.1, 0.2, and 0.3) are used to calibrate the model, the dash line shows the initial pdf, and the solid lines indicate the calibrated ones at the three time steps respectively.

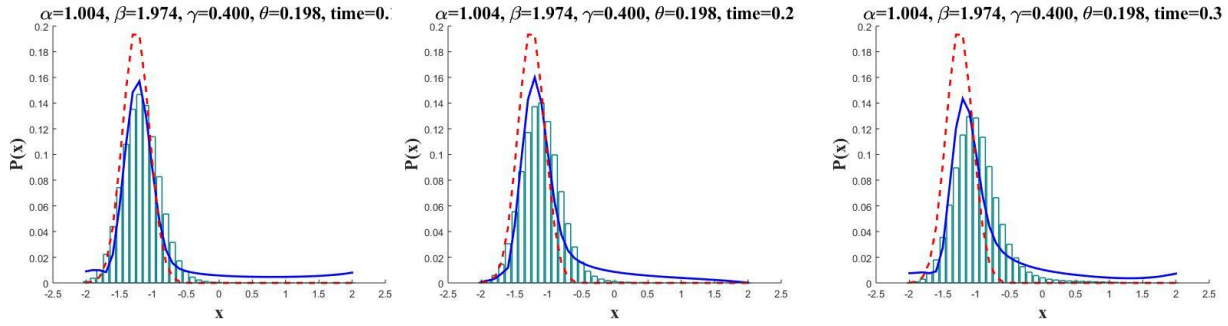

(a) (b) (c)

Figure 10: pdf's at three time steps are calibrated simultaneously against histograms of a diffusion process based on accumulative mutual information. (a) time step t=0.1. (b) time step t=0.2. (c) time step t=0.3.

5. DISCUSSIONS AND CONCLUSION

The method to quantify model-form uncertainty in simulating drift-diffusion phenomena is generic enough to capture the advection-diffusion and probability evolution driven by complex physical mechanisms. Therefore, the modeled processes are not restricted to Gaussian any more. Long-range correlations and memory effects are commonly observed in physical world. The simplification involved in Gaussian process modeling has inherent errors in its description. Fractional calculus provides a versatile tool to quantify and reduce the model-form uncertainty.

Except for a few simple pdf's that have analytical forms subject to fractional operators, most of fractional integrals and derivatives have to rely on numerical approaches to estimate. Fractional derivatives can be approximated by series of integer-order derivatives [36, 3], integer-order moments [37, 38], or finite difference [12]. The general analytical solution provided in Section 3 enables us to employ other numerical methods to find the solution. Numerical method is not the focus of this paper. Yet the approximated solutions obtained in the paper are based on fast Fourier transform with relatively low computational costs.

It is seen in Section 4.2 that the model calibration works well for some classical distributions. However, it should be aware that the four model-form parameters are not completely independent. It leads to the possibility that multiple optimum combinations of parameters produce the same distributions. This issue will become less apparent when multiple time steps of probability evolution are involved in the calibration process.

In the future work, numerical methods to enhance both the efficiency and accuracy for approximated solutions need to be studied. The discretization in real and reciprocal spaces for fast Fourier transform requires a large number of values to reduce the approximation error. A combination of approximations in real and functional spaces may improve the efficiency by reducing the density of discretization. How to incorporate multiple time steps efficiently in model calibration also requires more investigation.

REFERENCES

[1] Xiu, D. (2010). *Numerical Methods for Stochastic Computations: A Spectral Method Approach*, Princeton: Princeton University Press.

[2] Ghanem, R. G., & Spanos, P. D. (1991). *Stochastic finite elements: a spectral approach*. New York: Springer-Verlag.

[3] Samko, S. G., Kilbas, A. A., & Marichev, O. I. (1993). *Fractional Integrals and Derivatives: Theory and Applications*. Gordon and Breach Science Publishers, Yverdon.

[4] Miller, K. S., & Ross, B. (1993). *An introduction to the fractional calculus and fractional differential equations*. Wiley Interscience.

[5] Monje, C. A., Chen, Y., Vinagre, B. M., Xue, D., & Feliu-Batlle, V. (2010). *Fractional-order systems and controls: fundamentals and applications*. Springer, London.

[6] Tenreiro Machado, J. A., Silva, M. F., Barbosa, R. S., Jesus, I. S., Reis, C. M., Marcos, M. G., & Galhano, A. F. (2010). Some applications of fractional calculus in engineering. *Mathematical Problems in Engineering*, 2010, 639801.

[7] Sheng, H., Chen, Y., & Qiu, T. (2011). *Fractional processes and fractional-order signal processing: techniques and applications*. Springer, London.

[8] Carpinteri, A., Chiaia, B., & Cornetti, P. (2003). On the mechanics of quasi-brittle materials with a fractal microstructure. *Engineering Fracture Mechanics*, **70**(16), 2321-2349.

[9] Lazopoulos, K. A. (2006). Non-local continuum mechanics and fractional calculus. *Mechanics Research Communications*, **33**(6), 753-757.

[10] Fogedby, H. C. (1994). Lévy flights in random environments. *Physical Review Letters*, **73**(19), 2517-2520.

[11] Mainardi, F., Luchko, Y., & Pagnini, G. (2001). The fundamental solution of the space-time fractional diffusion equation. *Fractional Calculus and Applied Analysis*, **4**(2), 153-192.

[12] Liu, Q., Liu, F., Turner, I.W., & Anh, V.V. (2007). Approximation of the Lévy–Feller advection–dispersion process by random walk and finite difference method. *Journal of Computational Physics*, **222**(1), 57-70.

[13] Cottone, G., & Di Paola, M. (2009). On the use of fractional calculus for the probabilistic characterization of random variables. *Probabilistic Engineering Mechanics*, **24**(3), 321-330.

[14] Cottone, G., Di Paola, M., & Metzler, R. (2010). Fractional calculus approach to the statistical characterization of random variables and vectors. *Physica A: Statistical Mechanics and its Applications*, **389**(5), 909-920.

[15] Di Paola, M., & Pinnola, F. P. (2012). Riesz fractional integrals and complex fractional moments for the probabilistic characterization of random variables. *Probabilistic Engineering Mechanics*, **29**, 149-156.

[16] Di Matteo, A., Di Paola, M., & Pirrotta, A. (2014). Poisson white noise parametric input and response by using complex fractional moments. *Probabilistic Engineering Mechanics*, **38**, 119-126.

[17] Di Paola, M. (2014). Fokker Planck equation solved in terms of complex fractional moments. *Probabilistic Engineering Mechanics*, **38**, 70-76.

[18] Laskin, N. (2000). Fractional quantum mechanics and Lévy path integrals. *Physics Letters A*, **268**(4), 298-305.

[19] Jenkinson, A. F. (1955). The frequency distribution of the annual maximum (or minimum) values of meteorological elements. *Quarterly Journal of the Royal Meteorological Society*, **81**(348), 158-171.
[20] Hosking, J. R. M., Wallis, J. R., & Wood, E. F. (1985). Estimation of the generalized extreme-value distribution by the method of probability-weighted moments. *Technometrics*, **27**(3), 251-261.
[21] Wyss, W. (1986). The fractional diffusion equation. *Journal of Mathematical Physics*, **27**(11), 2782-2785.
[22] Meerschaert, M. M., Benson, D. A., & Bäumer, B. (1999). Multidimensional advection and fractional dispersion. *Physical Review E*, **59**(5), 5026-5028.
[23] Benson, D. A., Wheatcraft, S. W., & Meerschaert, M. M. (2000). The fractional-order governing equation of Lévy motion. *Water Resources Research*, **36**(6), 1413-1423.
[24] Metzler, R., Barkai, E., & Klafter, J. (1999). Deriving fractional Fokker-Planck equations from a generalised master equation. *Europhysics Letters*, **46**(4), 431-436.
[25] Liu, F., Anh, V. V., Turner, I., & Zhuang, P. (2003). Time fractional advection-dispersion equation. *Journal of Applied Mathematics and Computing*, **13**(1-2), 233-245.
[26] Huang, F., & Liu, F. (2005). The fundamental solution of the space-time fractional advection-dispersion equation. *Journal of Applied Mathematics and Computing*, **18**(1-2), 339-350.
[27] Liu, F., Zhuang, P., Anh, V., Turner, I., & Burrage, K. (2007). Stability and convergence of the difference methods for the space–time fractional advection–diffusion equation. *Applied Mathematics and Computation*, **191**(1), 12-20.
[28] Yıldırım, A., & Koçak, H. (2009). Homotopy perturbation method for solving the space–time fractional advection–dispersion equation. *Advances in Water Resources*, **32**(12), 1711-1716.
[29] Meerschaert, M. M., & Tadjeran, C. (2004). Finite difference approximations for fractional advection–dispersion flow equations. *Journal of Computational and Applied Mathematics*, **172**(1), 65-77.
[30] Jafari, H., & Momani, S. (2007). Solving fractional diffusion and wave equations by modified homotopy perturbation method. *Physics Letters A*, **370**(5), 388-396.
[31] Chechkin, A., Gonchar, V., Klafter, J., Metzler, R., & Tanatarov, L. (2002). Stationary states of non-linear oscillators driven by Lévy noise. *Chemical Physics*, **284**(1), 233-251.
[32] Alotta, G., & Di Paola, M. (2015). Probabilistic characterization of nonlinear systems under α-stable white noise via complex fractional moments. *Physica A: Statistical Mechanics and its Applications*, **420**, 265-276.
[33] Saltelli, A., Ratto, M., Andres, T., Campolongo, F., Cariboni, J., Gatelli, D., Saisana, M., and Tarantola, S., (2008) *Global Sensitivity Analysis: The Primer*. Wiley-Interscience
[34] Hu, J., Wang, Y., Cheng, A., & Zhong, Z. (2015) Sensitivity analysis in quantified interval constraint satisfaction problems. *Journal of Mechanical Design*, **137**(4), 041701.
[35] Gorenflo, R., Loutchko, J., and Luchko, Y. (2002) Computation of the Mittag-Leffler function $E_{\alpha,\beta}(z)$ and its derivative. *Fractional Calculus and Applied Analysis*, **5**(4), 491-518.
[36] Atanacković, T. M., Konjik, S., & Pilipović, S. (2008). Variational problems with fractional derivatives: Euler–Lagrange equations. *Journal of Physics A: Mathematical and Theoretical*, **41**(9), 095201.

[37] Djordjevic, V. D., & Atanackovic, T. M. (2008). Similarity solutions to nonlinear heat conduction and Burgers/Korteweg–deVries fractional equations. *Journal of Computational and Applied Mathematics*, **222**(2), 701-714.
[38] Pooseh, S., Almeida, R., & Torres, D. F. (2013). Numerical approximations of fractional derivatives with applications. *Asian Journal of Control*, **15**(3), 698-712.

List of Figures

List of Tables